Techset Composition Ltd, Salisbury
Doc: //techsetserver2/journal/IEE/RPG/Articles/pagination/RPGSI20150036_B&W.3d

IET Renewable Power Generation

Research Article

Sensorless control of a power converter for a cluster of small wind turbines

ISSN 1752-1416
Received on 27th January 2015
Revised on 24th November 2015
Accepted on 4th January 2016
doi: 10.1049/iet-rpg.2015.0036
www.ietdl.org

Agustí Egea-Alvarez[1,2] ✉, Mónica Aragüés-Peñalba[2], Oriol Gomis-Bellmunt[2,3], Joan Rull-Duran[4], Antoni Sudrià-Andreu[2]

[1]*Power system Department, China Electric Power Research Institute, No 15. Xiaoying East Road, 100192 Qinghe, Beijng, People's Republic of China*
[2]*Electrical Engineering Department, CITCEA-UPC, Technical University of Catalonia, Diagonal 647 Planta 2, Barcelona, Spain*
[3]*Electrical Engineering Area, Catalonia Institute for Energy Research (IREC), Jardins de Dones de Negre 1, 08963 Sant Adrià de Besòs, Barcelona, Spain*
[4]*Electrical Engineering Department, Technical University of Catalonia, Diagonal 647 Planta 2, Barcelona, Spain*
✉ *E-mail: agusti.egea@citcea.upc.edu*

Abstract: This study presents a new sensorless control for small wind turbine clusters with a single power converter with a direct torque control) algorithm. The proposed system consists of a wind farm connected to a back-to-back power converter that interfaces the wind farm with the AC grid. The studied wind turbines are based on fixed-speed wind turbines equipped with squirrel cage induction generators with individual pitch control. The presented structure permits to reduce the number of converters and allows to accomplish the grid codes (fault ride through capability and reactive power support). Furthermore, the generated active power can be reduced according to grid operator requirements. The presented control scheme can be applied to wind turbine repowering projects, wind farms connected to a microgrid, even, new small onshore and offshore power plants. The system performance and stability is studied and validated by means of dynamic simulations.

1 Introduction

Nowadays, there are several wind farms based on fixed-speed wind turbines concept connected to the AC grid. These wind farms were built during the 80s and 90s and represent the first generation of industrialised wind turbines [1]. In 1995, the installation of fixed speed wind turbines represented around 70% of the market share, in 2004 it only represented 32% [1].

Around 20–25 years after the first connection of the wind farm, the investment is fully recovered and some components are worn down. However, these wind turbines can have a second life after an exhaustive revision and replacement of the damaged components. This process is known as repowering. However, these wind turbines cannot be reconnected directly to the grid due to the evolution of the grid codes [2, 3].

Currently, a certain level of grid support is required, such as fault right through capability or reactive power support. To achieve these objectives, a power converter is needed. A standard solution is the installation of an individual power converter for each wind turbine. A cheaper and more feasible alternative consists of the installation of a single power converter in a back-to-back structure for the entire wind farm. Since the wind turbines are close to each other, the wind speed can be assumed to be in the same range for all the different wind turbines [4].

The individual control of a squirrel cage induction generator (SCIG) has been widely discussed in the literature. The two most used control techniques are the flux oriented control [5, 6] (FOC) and the direct torque control [7, 8] (DTC). Both systems present independent control of torque and flux with high-performance results. However, the FOC needs to be oriented in its basic implementation (an extra speed/position sensor is required) while the DTC is a sensorless method (it only requires electrical measures). However at the same time, FOC provides a smooth torque response whereas the DTC presents a torque ripple. For this reason, DTC is recommended for high inertia applications.

There are several authors who present energetic studies and electrical control for wind farms with a single power converter [9–12]. The main advantages of this approach compared with the classic approach – a single converter per wind turbine – are lower maintenance costs, higher reliability and efficiency thanks to the reduced number of components. In [11, 12], the concept of a wind farm based on SCIG and synchronous generator are presented using a single power converter. Another control approach based on scalar control is presented in [10].

In this paper, a new wind farm control with a centralised power converter based on DTC multimachine algorithm is presented and discussed for a small wind farm. This structure permits to adapt old wind farms equipped with SCIG to new grid codes and also it allows to control new small wind turbines connected to the main AC grid or a microgrid. This paper is structured as follows: first, the analysed system and model equations are presented. Later, the operation modes and the control scheme are described. Finally, the system efficiency and stability are verified and some dynamic simulations are performed.

2 Analysed system

The analysed system is a small wind farm cluster composed of several wind turbines based on fixed-speed SCIG with individual pitch control. Each wind turbine drive train is composed of the wind turbine, a gearbox and an SCIG. There is a single back-to-back power converter that interfaces the wind farm with the AC grid. Also, there is a DC chopper in the DC bus to dissipate power during an AC contingency. A sketch of the analysed topology can be seen in Fig. 1.

3 Control scheme

3.1 Wind turbine model

The wind turbine has been modelled using a C_p mathematical approach, where the power extracted from the wind (P_{tur}) is

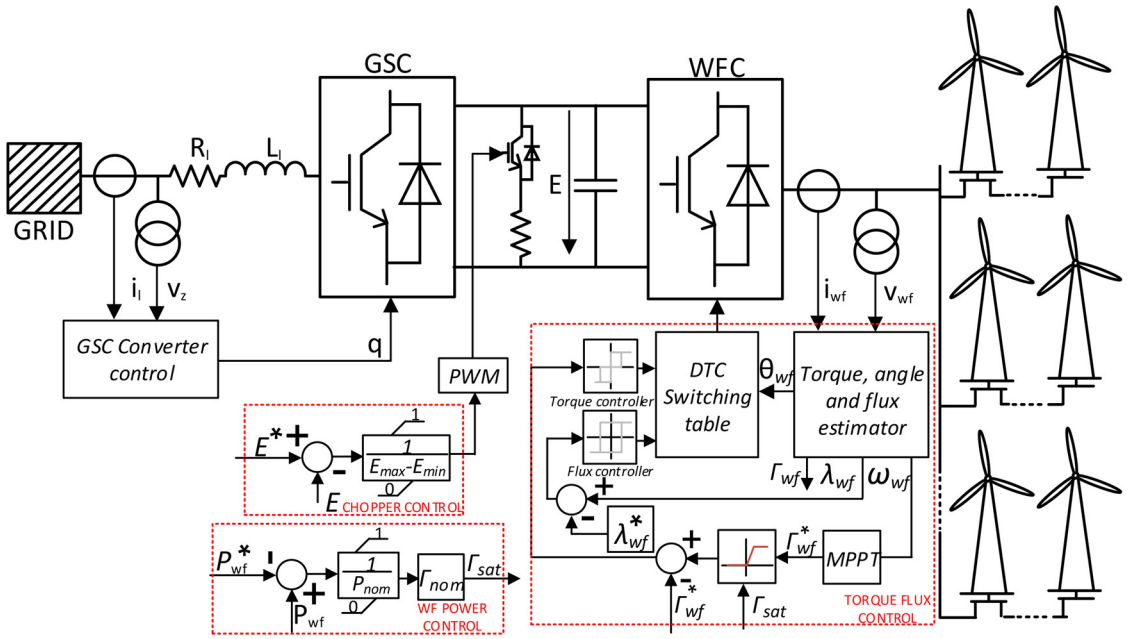

Fig. 1 *Power and control scheme of the proposed control system*

calculated as

$$P_{\text{tur}} = \frac{1}{2}\rho\pi R^2 C_p v_{\text{wind}}^3 \tag{1}$$

where C_p is the power coefficient, R is the wind turbine radius and ρ is the air density. C_p is defined as [13]

$$C_p = C_1\left(C_1\frac{1}{\Lambda} - C_3\theta_{\text{pitch}} - C_4\theta_{\text{pitch}}^{c5} - C_6\right)e^{(-c_7/\Lambda)} \tag{2}$$

$$\frac{1}{\Lambda} = \frac{1}{\lambda + c_8\theta_{\text{pitch}}} - \frac{c_9}{1+\theta_{\text{pitch}}^3} \tag{3}$$

$$\lambda = \frac{\omega_{\text{tur}}R}{v_{\text{wind}}} \tag{4}$$

where $C_{1..9}$ are the power coefficients, θ_{pitch} is the pitch angle, R is the wind turbine rotor radius, ω_{tur} is the rotational speed of the wind turbine and v_{wind} is the wind speed. The torque developed by the wind turbine (Γ_{tur}) is

$$\Gamma_{\text{tur}} = \frac{P_{\text{tur}}}{\omega_{\text{tur}}} \tag{5}$$

3.2 Electrical system model

The electrical system is composed of the SCIG, the AC cables and the power converter. The SCIG equations used are as follows [14]

$$v_{ds} = R_s i_{ds} + \frac{\mathrm{d}\lambda_{ds}}{\mathrm{d}t} - \omega\lambda_{qs} \tag{6}$$

$$v_{qs} = R_s i_{qs} + \frac{\mathrm{d}\lambda_{qs}}{\mathrm{d}t} + \omega\lambda_{ds} \tag{7}$$

$$v_{dr} = R_r i_{dr} + \frac{\mathrm{d}\lambda_{dr}}{\mathrm{d}t} - (\omega - \omega_r)\lambda_{qs} \tag{8}$$

$$v_{qr} = R_r i_{qr} + \frac{\mathrm{d}\lambda_{qr}}{\mathrm{d}t} + (\omega - \omega_r)\lambda_{dr} \tag{9}$$

where, v is the voltage at electrical machine terminals, i is the current across the stator, R is the resistance, ω_r is the rotational speed, ω is the electrical speed and λ is the flux. The subscript q and d refer to the stationary reference frame components and s and r refer to stator and rotor, respectively. The fluxes are expressed as

$$\lambda_{ds} = L_{ls}i_{ds} + L_m(i_{ds} + i_{dr}) \tag{10}$$

$$\lambda_{qs} = L_{ls}I_{qs} + L_m\left(i_{qs} + i_{qr}\right) \tag{11}$$

$$\lambda_{dr} = L_{lr}I_{dr} + L_m\left(i_{ds} + i_{dr}\right) \tag{12}$$

$$\lambda_{qs} = L_{lr}I_{qr} + L_m\left(i_{qs} + i_{qr}\right) \tag{13}$$

where L_{lr} is the rotor self-inductance, L_{ls} is the stator self-inductance and L_m is the magnetising inductance. The torque developed by the electrical machine is

$$\Gamma_{\text{ele}} = \frac{3P}{2}(i_{qs}\lambda_{ds} - i_{ds}\lambda_{qs}) \tag{14}$$

The cables have been modelled as impedance

$$Z_{\text{cable}} = R_{\text{cable}} + \mathrm{j}X_{\text{cable}} \tag{15}$$

The back-to-back has been modelled as a detailed two level voltage source converter [including insulated-gate bipolar transistors (IGBTs)]. The DC chopper has been modelled as a resistance with a series IGBT and the AC grid has been modelled as a Thevenin equivalent.

3.2 Gearbox and transmission model

The wind turbine is connected to the electric machine using a gearbox to match the rotational speed of both, the wind turbine and the electrical machine. It is modelled as a first order system as

$$\Gamma_{\text{tur}} - \Gamma_{\text{ele}}\nu = J_{\text{total}}\frac{\mathrm{d}\omega_{\text{tur}}}{\mathrm{d}t} \tag{16}$$

where J_{total} is the wind turbine inertia and ν is the gearbox ratio.

4 Control system

4.1 General overview and operation model

Q1 The control system is divided into two parts: the GSC control and the WFC control. A control overview can be seen in Fig. 1. The GSC control is in charge of the DC voltage and the reactive power injected to the grid. It also controls the DC chopper used to dissipate the exceeded power during an AC contingency. The WFC control is in charge of the torque and the flux of the whole wind farm solely using electrical measures. A DTC-based algorithm is used because of its inherent sensorless capability and its high dynamic performance. The wind farm operation can be divided into three different states:

- *Normal operation:* When the wind speed is under the nominal value the system extracts the maximum power available. The maximum power point tracking (MPPT) calculates the maximum power that can be extracted from the wind according to the estimated rotational speed and the DTC-based algorithm drives the wind turbine to the optimal operational point. Consequently, in this mode the electrical frequency of the AC grid adapts to work at the optimal operational point. If the nominal wind is reached, the reference torque of the system is kept constant and the wind turbine pitch control system starts to reduce the power extracted from the wind.
- *AC grid fault:* During an AC contingency, probably all the generated power will not be injected to the grid due to the saturation of the GSC AC current. In this case, the energy starts to be stored in the DC bus and the voltage starts to rise. The presented topology is equipped with a DC chopper that can dissipate this energy when the DC voltage is above the nominal maximum voltage. Using a DC chopper during grid contingencies, wind turbines do not suffer the effects of the AC contingencies. Once the AC grid is recovered the GSC returns to the previous operation point.
- *Power reduction reference:* In some circumstances, the grid operator may require an active power reduction. To reach the desired power level, the WFC control adapts the torque reference saturation to reduce the generated power. When the torque is reduced, the wind turbines accelerate and the pitch control adapts the captured power to match the power demanded by the grid operator. In normal operation, the wind farm power reference (P^*_{wf}) is set to its nominal value (P_{nom}).

4.2 Wind farm converter control

The WFC control is based on a DTC control algorithm for SCIG adapted for multimachine schemes (Fig. 1). A flux, torque and speed wind farm equivalent are used instead of the individual machine variables. The DTC control algorithm is composed of the wind farm equivalent torque estimator, the wind farm equivalent flux (angle and magnitude) estimator, the average rotational speed estimator, the hysteresis controllers and the DTC switching tables. The estimator is the part of the control system where the non-measured variables are calculated; its schematic is presented in Fig. 2. The equivalent wind farm flux (λ_{wf}) is calculated as

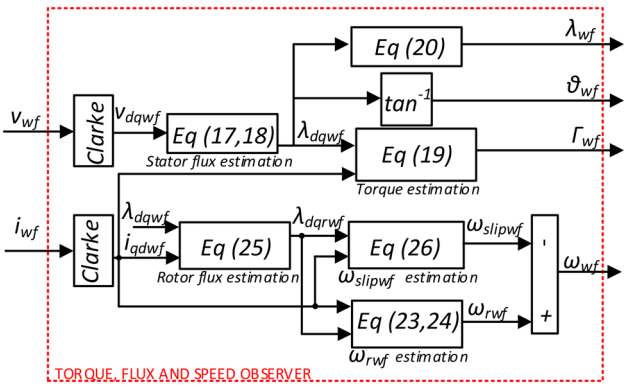

Q **Fig. 2** *Torque, flux and speed observer*

$$\lambda_{d\mathrm{wf}} = \left(v_{d\mathrm{wf}} - R_{\mathrm{wf}} i_{d\mathrm{wf}}\right) \mathrm{d}t \tag{17}$$

$$\lambda_{q\mathrm{wf}} = \left(v_{q\mathrm{wf}} - R_{\mathrm{wf}} i_{q\mathrm{wf}}\right) \mathrm{d}t \tag{18}$$

where R_{wf} is the equivalent resistance of the electrical wind farm grid at the power converter terminals, i_{wf} is the AC current flowing across the WFC and v_{wf} is the voltage at AC WFC terminals. Once the d and q components are calculated, it is possible to calculate the wind farm electrical torque (Γ_{wf}) as

$$\Gamma_{\mathrm{wf}} = \frac{3P}{2}\left(i_{q\mathrm{wf}}\lambda_{d\mathrm{wf}} - i_{d\mathrm{wf}}\lambda_{q\mathrm{wf}}\right) \tag{19}$$

where that wind farm flux magnitude is

$$\lambda_{\mathrm{wf}} = \sqrt{\lambda^2_{d\mathrm{wf}} + \lambda^2_{q\mathrm{wf}}} \tag{20}$$

and the average wind farm flux angle needed to determine the appropriate switching vector is

$$\theta_{\mathrm{wf}} = \tan^{-1}\left(\frac{\lambda_{q\mathrm{wf}}}{\lambda_{d\mathrm{wf}}}\right) \tag{21}$$

The average rotational speed (ω_{wf}) is needed by the MPPT to determine the optimal wind farm power extraction. Since there is no speed sensor, the rotational speed of the wind farm is estimated as

$$\omega_{\mathrm{wf}} = \omega_{\mathrm{rwf}} - \omega_{\mathrm{slipwf}} \tag{22}$$

where, ω_{rwf} is the average electric angular velocity and ω_{slipwf} is the average slip angular velocity. To calculate the average speed, the i_{wf} is divided by the number of wind turbines (N_{wf}). The electrical speed is determined from the wind farm equivalent rotor flux as

$$\omega_{\mathrm{rwf}} = \frac{\mathrm{d}\theta_{\mathrm{rwf}}}{P\,\mathrm{d}t} \tag{23}$$

where P is the number of pole pairs and θ_{rwf} is

$$\theta_{\mathrm{rwf}} = \tan^{-1}\left(\frac{\lambda_{q\mathrm{rwf}}}{\lambda_{d\mathrm{rwf}}}\right) \tag{24}$$

the rotor equivalent flux amplitude and angle are calculated as

$$\begin{aligned}\lambda_{\mathrm{rwf}} &= \sqrt{\lambda^2_{d\mathrm{rwf}} + \lambda^2_{q\mathrm{rwf}}} \\ &= \sqrt{\left(\frac{L_{\mathrm{r}}}{L_{\mathrm{m}}}\left(\lambda_{d\mathrm{wf}} - \sigma L_{\mathrm{s}}\frac{i_{d\mathrm{wf}}}{N_{\mathrm{wt}}}\right)\right)^2 + \left(\frac{L_{\mathrm{r}}}{L_{\mathrm{m}}}\left(\lambda_{q\mathrm{wf}} - \sigma L_{\mathrm{s}}\frac{i_{q\mathrm{wf}}}{N_{\mathrm{wt}}}\right)\right)^2}\end{aligned} \tag{25}$$

where $\sigma = 1 - (L^2_{\mathrm{m}}/L_{\mathrm{s}}L_{\mathrm{r}})$. The average slip angular velocity is expressed as

$$\omega_{\mathrm{slipwf}} = \frac{(R_{\mathrm{r}}L_{\mathrm{m}}/L_{\mathrm{r}})\left(\lambda_{q\mathrm{rwf}} i_{d\mathrm{wf}} - \lambda_{d\mathrm{rwf}} i_{q\mathrm{wf}}\right)}{\lambda^2_{\mathrm{wf}}} \tag{26}$$

Once all the needed variables are estimated, applying the DTC algorithm is possible. The DTC consists of applying a given voltage vector depending on the flux/torque hysteresis controller outputs and the sector. The flux hysteresis controller has two possible states and the torque controller has three possible output states. The DTC switching tables used in this paper are extracted from [15]. The optimum torque reference is calculated using an open loop MPPT [16] algorithm based on the wind turbine physical

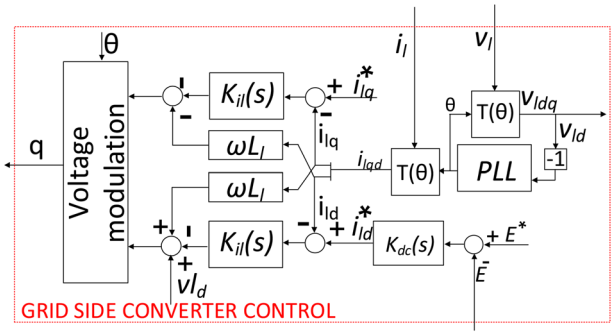

Fig. 3 *GSC control scheme*

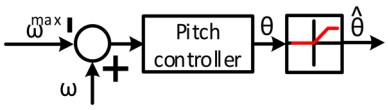

Fig. 4 *Pitch angle controller*

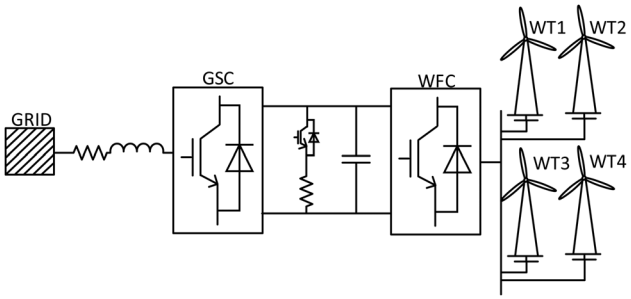

Fig. 5 *Scheme of the studied system*

characteristics. It is defined as

$$\Gamma^* = \frac{(1/2)\rho A R^3 \omega_{\mathrm{wf}} \left(c_1 \, \mathrm{e}^{-(c_6 c_7 + c_2/c_2)} \left(c_2 c_7 c_9 + c_6 c_7 + c_2 \right)^3 \right)}{c_2^2 c_7^4} \tag{27}$$

as all the terms are constant except the wind turbine rotational speed. It can be simplified as

$$\Gamma^* = k_{c_p}^2 \, \omega_{\mathrm{wf}} N_{\mathrm{wt}} \tag{28}$$

The torque reference is limited once the system reaches the nominal torque. Past this point, the torque reference is set as constant. As the grid operator may require a power reduction, [17] the torque saturation (Γ_{sat}) is modified accordingly to deliver the required power as

$$\Gamma^{\mathrm{sat}} = \frac{\left(P_{\mathrm{nom}} - P_{\mathrm{wf}}^* \right)}{P_{\mathrm{nom}}} \frac{\Gamma_{\mathrm{nom}}}{T_s s + 1} \tag{29}$$

where Γ_{nom} is the nominal torque and T_s is the first order filter time constant used to filter the power reduction effect. This control implementation can be seen in Fig. 1 as WF power control.

4.3 Grid side converter control and DC chopper control

The GSC regulates the DC bus voltage and the reactive power exchanged with the AC main grid independently. A sketch of the control system can be seen in Fig. 3. The implemented control strategy is based on an inner current control and an outer DC voltage control. At the same time, a PLL is needed to track the AC grid phase. The current control is composed by two proportional–integral (PI) controllers, one for each component in the synchronous reference frame, and a decoupling feed-forward. The inner current control PI controller is

$$K_{\mathrm{il}}(s) = \frac{K_{\mathrm{iil}} s + K_{\mathrm{pil}}}{s} = \frac{(R_l/\alpha)s + (L_l/\alpha)}{s} \tag{30}$$

where K_{iil} and K_{pil} are the inner loop integral and proportional gains and R_l and L_r are the resistance and the inductance of the coupling filter. The DC voltage control is based on a PI controller as

$$K_{\mathrm{dc}}(s) = \frac{K_{\mathrm{pdc}} s + K_{\mathrm{pdc}}}{s} \tag{31a}$$

where K_{idc} and K_{pdc} are the integral and proportional gains of the DC voltage regulator.

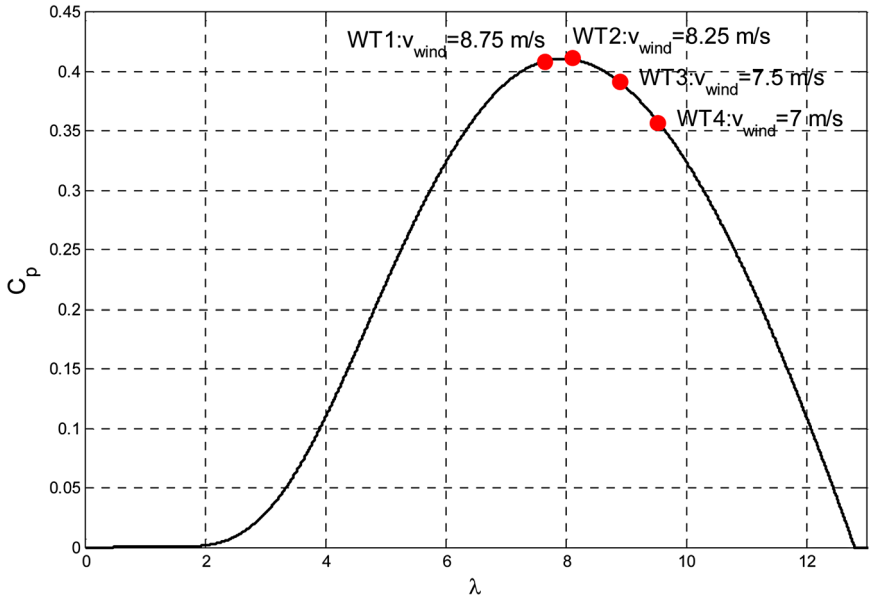

Fig. 6 *Operating C_p for the different wind speeds*

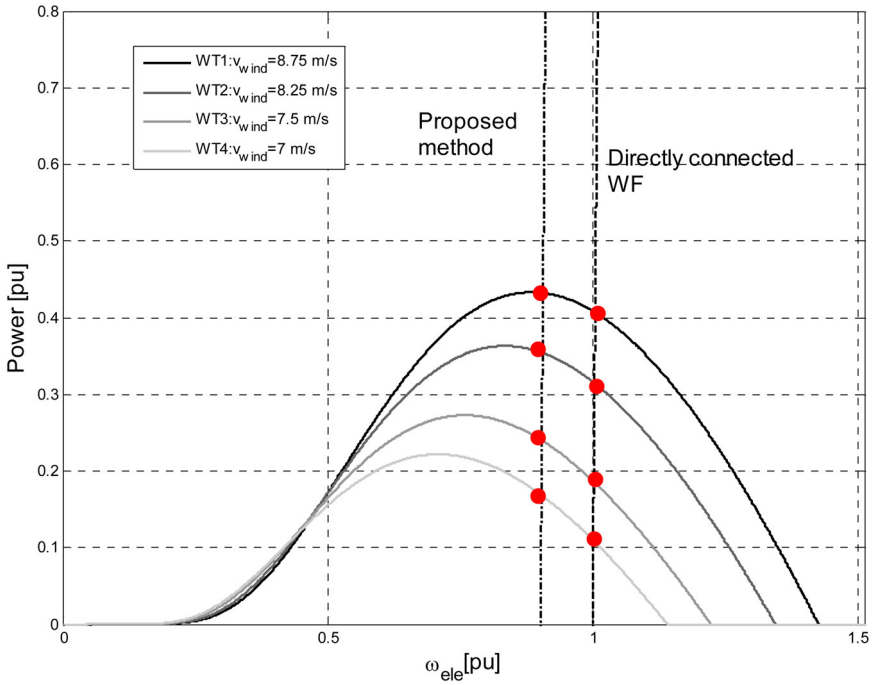

Fig. 7 *Power curve for the different wind turbines considering that the machines are directly connected or connected using the proposed method*

Table 1 Eigenvalues of the wind turbines

	Wind turbine 1	Wind turbine 2	Wind turbine 3	Wind turbine 4
electric pole 1	−62.90 + j 306.13	−62.90 + j 306.12	−62.90 + j 306.11	−62.91 + j 306.10
electric pole 2	−62.90 − j 306.13	−62.90 − j 306.12	−62.90 − j 306.11	−62.91 − j 306.10
electric pole 3	−31.99 + j 63.19	−32.03 + j 63.48	−32.09 + j 63.93	−32.13 + j 64.23
electric pole 4	−31.99 − j 63.19	−32.03 − j 63.48	−32.09 − j 63.93	−32.13 − j 64.23
transmission pole	−4.37	−4.30	−4.20	−4.12

The DC chopper is controlled by means of the IGBT duty cycle. The used control law is a proportional controller described as

$$d = \frac{E_{\min} - E}{E_{\max} - E_{\min}} \tag{31b}$$

where $E_{\min}$ is the minimum voltage chopper threshold, $E_{\max}$ is the maximum voltage chopper threshold and E is the DC voltage value. The DC chopper controller output is saturated between 0 (no chopper actuation) and 1 (DC chopper is fully connected)

4.4 Wind turbine pitch control

Each wind turbine has an individual pitch control system that is actioned when the wind speed is higher than the referenced value ($\omega^{\max}$). In the studied system, this value matches the nominal speed when the machine is acting as a generator. A sketch of the pitch control can be seen in Fig. 4. The system is tuned as following [18].

The pitch controller is implemented as a PI controller as

$$K_{\text{pitch}}(s) = \frac{K_{\text{ppitch}} s + K_{\text{ipitch}}}{s} \tag{32}$$

where K_{ppitch} and K_{ipitch} are the proportional and integral gains of the pitch controller

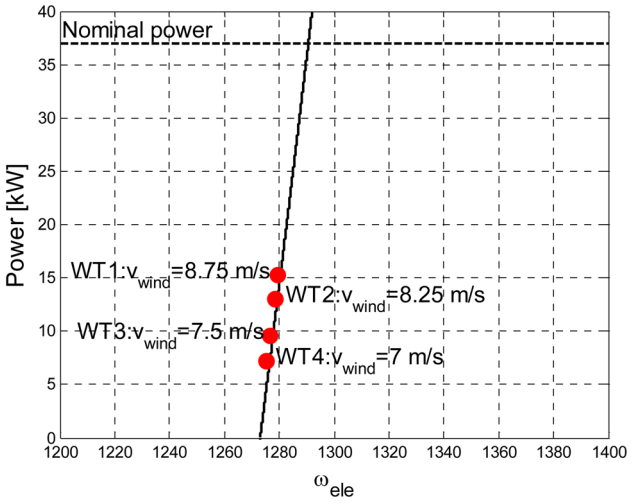

Fig. 8 *Steady-state electric characteristic of the induction machines with the operation working point for the different wind turbines*

5 Performance and stability analysis

In this section, the performance and the stability of the proposed system are analysed. A four wind turbine wind farm with a nominal power of 37 kW at $v_{\text{wind}}^{\text{nominal}} = 12$ m/s each is analysed. Each wind turbine is connected to the WFC busbar terminals using independent line (see Fig. 5). The wind turbine parameters used are: rotor radius (R) is 5.5 m, the air density (ρ) is 1.125 kg/m^3, the power coefficients are $c_{1..9} = 0.44$, 125, 0, 0, 0, 6.94, 16.5, 0, −0.002 and the gearbox ratio (n) is 11. The electrical machine parameters used are: $V_n = 400$ V, $P_n = 37$ kW, $\omega_n = 1518$ rpm, $R_s = 0.08233\ \Omega$, $L_s = 0.724$ mH, $R_r = 0.0503\ \Omega$, $L_r = 0.724$ mH, $L_m = 0.02711$ mH, $T_s = 0.5$ s, $K_{\text{ppitch}} = 2$, $K_{\text{ipitch}} = 5$, $K_{\text{idc}} = 100$ $K_{\text{pdc}} = 4$, $E_{\max} = 830$ V and $E_{\min} = 815$ V.

The system is analysed under four constant wind speeds: $v_{\text{WT1}} = 8.75$ m/s, $v_{\text{WT2}} = 8.25$ m/s, $v_{\text{WT3}} = 7.5$ m/s and $v_{\text{WT4}} = 7$ m/s. Usually, the wind speeds for wind turbines located near each other

are similar [4], but in this analysis they have been considered to be substantially different to prove the system robustness.

5.1 MPPT and system performance

The described MPPT in (27) is the optimum solution for a single or a group of wind turbines with identical wind speed. However, when it is used considering the average speed of the wind farm the MPPT calculates an average optimum torque for the whole wind farm [19]. Fig. 6 shows the λ–C_p characteristic for the analysed wind turbines, where the individual wind turbine operational point have been marked. As it can be seen, WT1 and WT2 are working near the maximum C_p and WT3 and WT4 are working with a less efficient C_p due to the wind speed difference.

If the power generated by the proposed system is compared with the power generated when the wind turbines are directly connected, the output power is 20% higher (see Fig. 7, the total power is the sum of the red dots). In the first case, the generated power is around 44 kW and in the second case, it is around 36.5 kW. As it can be seen in Fig. 7, as the proposed method can vary the system frequency, it is possible to adapt the rotational speed in order to capture more power.

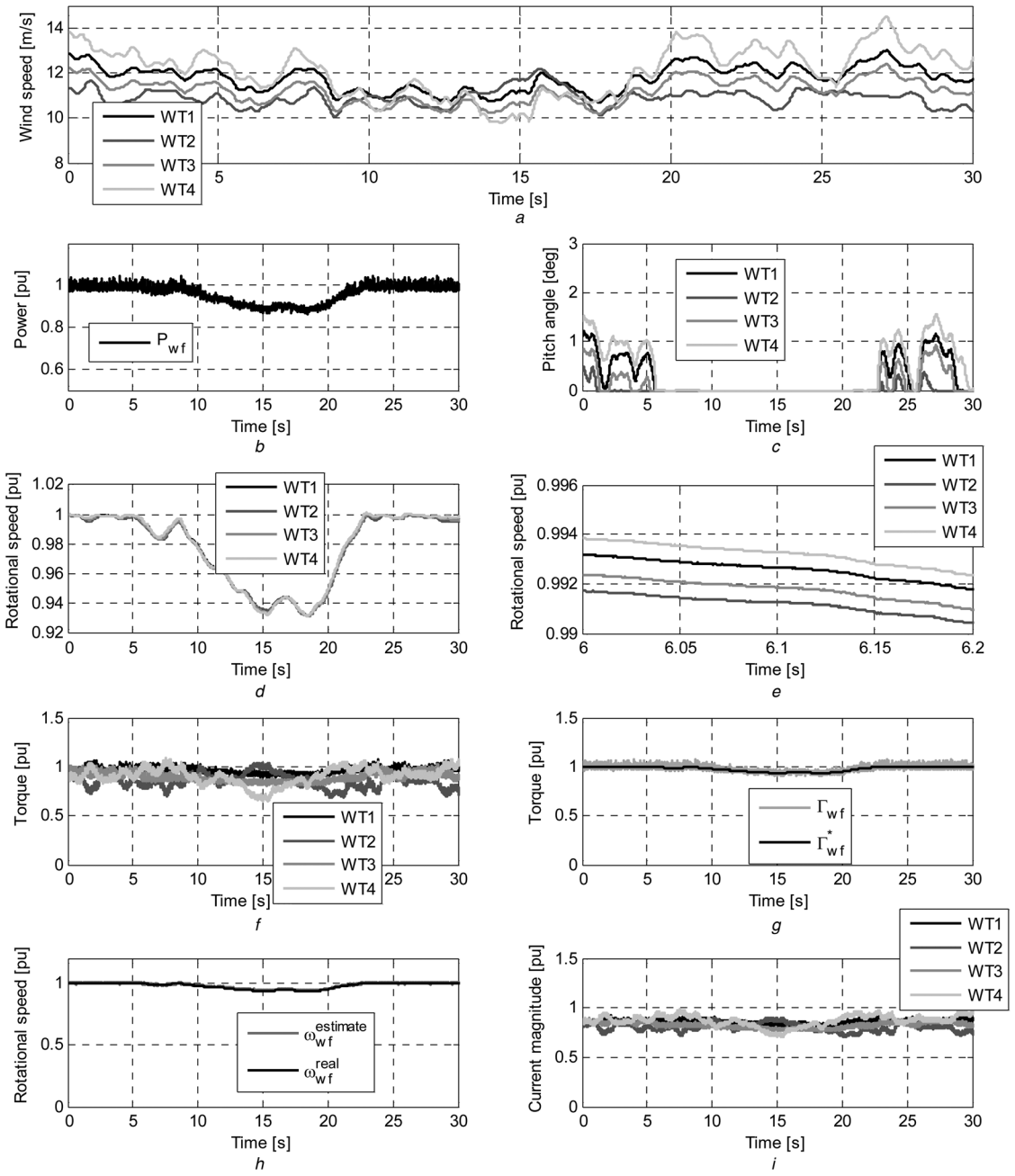

Fig. 9 *Wind series simulation*

a Wind speeds for the different wind turbines
b Generated active power
c Wind turbine pitch angles
d Individual wind turbine rotational speed
e Detailed rotational speed during 200 ms
f Individual wind turbine torque
g Wind farm average torque and reference
h Average and estimated wind farm rotational speed
i Current magnitude for each wind turbine

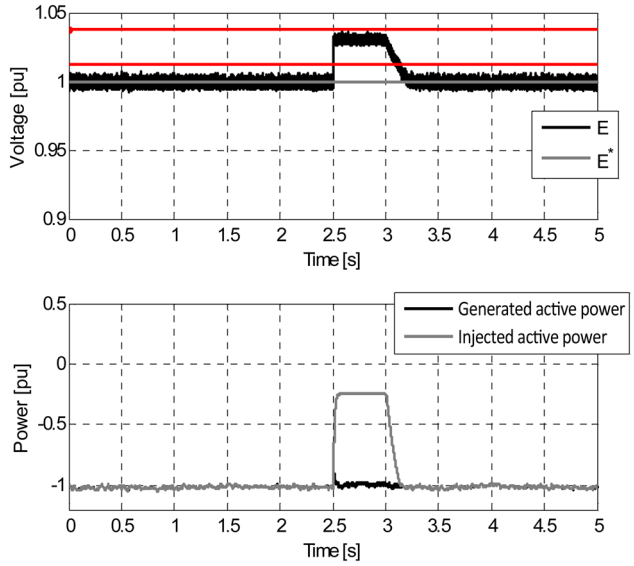

Fig. 10 *DC voltage evolution (in red the minimum (E_{min}) and maximum (E_{max}) thresholds) and active power generated and injected to the grid*

5.2 Stability of the proposed controller

The aim of this section is to show the stability of the proposed control structure. Due to the non-linear nature of the DTC, the classic control analysis tools cannot be used. In [20], the stability of the DTC is addressed in deep. In this paper, the stability of the whole wind farm is studied linearising the model and the DTC hysteresis controllers are considered stable. The wind turbine eigenvalues are calculated from the linearised model and presented in Table 1. As it can be observed, the electrical poles and the mechanical pole (transmission) are in the left-hand plane and the system is stable even if the electrical machines are rotating at different speeds due to the slip of the induction machines. This is an intrinsic phenomenon in induction machines. Fig. 8 shows the static characteristic power–speed curve of an induction machine with the different working points for the studied case.

6 Simulation results

In addition, the proposed control system is tested in a set of dynamic simulations. The first scenario consists in operation under varying wind speeds, the second is an AC voltage sag and the third is an

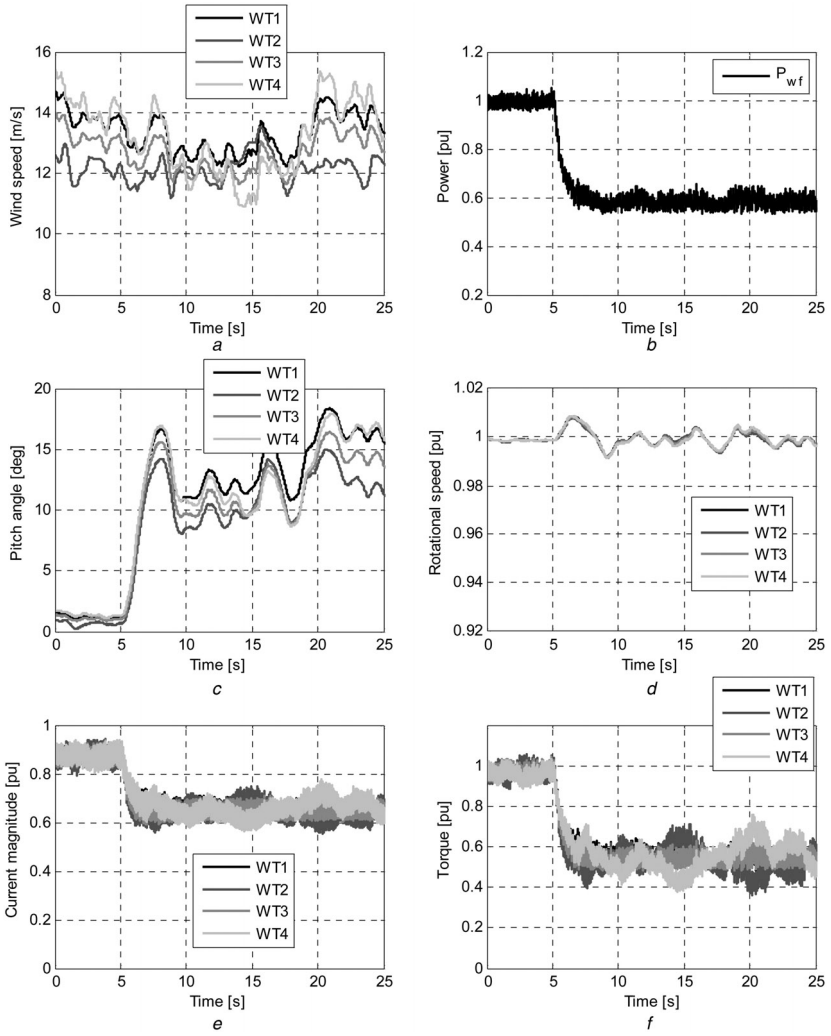

Fig. 11 *Active power reduction*

a Wind speed
b Active power
c Pitch angle
d Rotational speed
e Current magnitude
f Torque for each wind turbine

active power reference change. The simulations have been done using MATLAB/Simulink.

6.1 Wind series simulation

Fig. 9 shows the wind speeds for the different wind turbines (a), the active power (b), the pitch angle evolution (c), the individual wind turbine rotational speed (d) and (e) and torque (f), the estimated and reference wind farm torque (g), the estimated and real wind farm rotational speed (h) and the current magnitude (i) ($\cos\phi = 0.8$). During time instants $t = 0$ s and $t = 5$ s, the wind speed is above the nominal value and the system is keeping the torque reference at its maximum. Due to the wind turbine acceleration, the pitch control limits the rotational speed at its maximum value. During this period, the generated power is around 1 pu.

Between time instants $t = 5$ s and $t = 20$ s, the average wind speed is lower than the nominal wind speed and the MPPT changes the torque reference to extract the maximum power. After $t = 20$ s the system is saturated again and the active power is regulated using the pitch system.

The DTC control system is properly tracking the optimal torque reference and the average wind farm speed is being correctly estimated. The current for each wind turbine is less than the nominal current. The torque and the rotational speed of each wind turbine is below their nominal values, even when the wind is above the nominal value. In addition, details of the wind turbine rotational speeds between time instant $t = 6$ and 6.2 s shows the small differences due to the slip.

6.2 AC voltage sag

In this scenario, an AC voltage sag with a depth of 75% is simulated for the same wind profile described in the first scenario. Fig. 10 shows the DC voltage and active power generated in the wind farm and injected to the AC system. Before the voltage sag, the wind farm is delivering to the grid all the generated power. The voltage sag is applied at time instant $t = 2.5$ s. The GSC reaches the AC current limit. Consequently, the maximum amount of active power that can be injected in the AC grid is reduced up to 0.3 pu. During the first instants of the voltage sag, the DC voltage starts to rise and the minimum chopper threshold is crossed. Consequently, the DC chopper starts to dissipate power. Some milliseconds later, the DC chopper reaches an equilibrium point and the voltage is controlled at 1.03 pu. At time instant $t = 3$ s, the contingency is cleared and the grid voltage returns to its nominal value. At this moment, the DC chopper is disconnected and returns to the previous nominal voltage. During the voltage sag, the wind farm is generating the same amount of power as before.

6.3 AC power reduction

In this scenario, a 40% power reference reduction demanded by the grid operator is simulated. Fig. 11 shows the wind speed for the four wind turbines, the power generated by the wind farm, the individual pitch angle for each wind turbine, the rotational speed, current magnitude and torque for each wind turbine. At time instant $t = 5$ s, the power reference is reduced to 60% of its nominal value. Consequently, the generated power is reduced from near 1 to 0.6 pu following a first order response according to the time constant T_s. As there is an amount of power that cannot be injected to the AC system, the wind turbines start to accelerate and the power is controlled by the pitch angle. Consequently, after a small transient the system is able to control the active by means of pitch control. Compared with the first simulated scenario, as the needed power reduction is more aggressive the pitch angles are higher. During this transient the current, the torque or the speed do not exceed its limits.

7 Conclusion

This paper has introduced a sensorless control system for a small wind turbine cluster. This system is based on a DTC algorithm adapted for multimachine purposes and an MPPT system. The concept can be applied on small wind farm clusters (such as a repowering project, small wind farms built in rural areas or microgrids), but also in large wind power plants. The present structure can generate more power than the wind farm directly connected to the grid, thanks to the MPPT and the ability to change the electrical frequency. At the same time, the system stability has been proved through its linear model. The performance of the system during normal operation, AC contingencies and power reduction has been evaluated using three simulated cases: a steep wind change, an AC voltage sag and an active power reference change. The simulations have shown that the wind farm speed and torque are observed properly and the current, speed and torque are kept into the operation modes.

8 Acknowledgments

This work was funded by the Spanish Ministry of economy and competitiveness under the project number ENE2012-33043 and the European founded project MEDOW. The authors thank the English language correction done by Jordi Molero-Mora.

9 References

1 Hansen, A.D., Hansen, L.H.: 'Wind turbine concept market penetration over 10 years (1995.2004)', *Wind Energy*, 2007, **10**, pp. 81–87
2 Tsili, M., Papathanassiou, S.: 'A review of grid code technical requirements for wind farms', *IET Renew. Power Gener.*, 2009, **3**, (3), pp. 308–332
3 Mohseni, M., Syed, M.: 'Review of international grid codes for wind power integration: diversity, technology and a case for global standard', *Renew. Sustain. Energy Rev.*, 2012, **6**, pp. 3876–3890
4 Prada, M., Gomis-Bellmunt, O., Sumper, A., *et al.*: 'Analysis of a multi turbine offshore wind farm connected to a single large power converter operated with variable frequency', *Energy*, 2011, **36**, (5), pp. 3272–3281
5 Domínguez-García, J.L., Gomis-Bellmunt, O., Trilla-Romero, L., *et al.*: 'Indirect vector control of a squirrel cage induction generator wind turbine', *Comput. Math. Appl.*, 2012, **64**, (2), pp. 102–114
6 Rupprecht, G., Leonhard, W., Nordby, C.: 'Field-oriented control of a standard AC motor using microprocessors', *IEEE Trans. Ind. Appl.*, 1980, pp. 186–192
7 Nash, J.N.: 'Direct torque control, induction motor vector control without an encoder', *IEEE Trans. Ind. Appl.*, 1997, **33**, (2), pp. 333–341
8 Takahashi, I., Ohmori, Y.: 'High-performance direct torque control of an induction motor', *IEEE Trans. Ind. Appl.*, 1989, **25**, pp. 257–264
9 Prada, M., Gomis-Bellmunt, O., Sumper, A., *et al.*: 'Power generation efficiency analysis of offshore wind farms connected to a SLPC (single large power converter) operated with variable frequencies considering wake effects', *Energy*, 2012, **37**, (1), pp. 455–468
10 Trilla, L., Gomis-Bellmunt, O., Junyent-Ferré, A., *et al.*: 'Control of a squirrel cage induction generator wind farm connected to a single power converter'. Universities Power Engineering Conf. (UPEC), August 2010
11 Gomis-Bellmunt, O., Junyent-Ferré, A., Sumper, A., *et al.*: 'Control of a wind farm based on synchronous generators with a central HVDC-VSC converter', *IEEE Trans. Power Syst.*, 2011, **26**, (3), pp. 1632–1640
12 Egea-Alvarez, A., Junyent-Ferre, A., Bergas-Jané, J., *et al.*: 'Control of a wind turbine cluster based on squirrel cage induction generators connected to a single VSC power converter', *Int. J. Electr. Power Energy Syst.*, 2014, **61**, pp. 523–530
13 Ackermann, T.: 'Wind power in power systems' (Willey, 2012, 2nd edn.)
14 Krause, P.C., *et al.*: 'Analysis of electric machinery and drive systems' (John Wiley & Sons, 1995)
15 Vas, P.: 'Sensorless vector and direct torque control' (Oxford University Press, 1998)
16 Goodfellow, D., *et al.*: 'Control strategies for variable speed wind energy recovery'. Proc. of the Eighth BWEA Conf., Cambridge, UK, 1986
17 Hendriks, R.L., Velzke, R., Kling, W.L.: 'Fault ride-through strategies for VSC-connected wind parks'. European Wind Energy Conf., Marseille, France, 2009
18 Holdsworth, L., Charalambous, I., Ekanayake, J.B., *et al.*: 'Power system fault ride through capabilities of induction generator based wind turbines', *Wind Eng.*, 2004, **28**, (4)
19 Gomis-Bellmunt, O., Junyent-Ferré, A., Sumper, A., *et al.*: 'Maximum generation power evaluation of variable frequency offshore wind farms when connected to a single power converter', *Appl. Energy*, 2010, **87**, (10), pp. 3103–3109
20 Ortega, R., Barabanov, N., Escobar, G., *et al.*: 'Direct torque control of induction motors: stability analysis and performance improvement', *IEEE Trans. Autom. Control*, 2001, **46**, (8), pp. 1209–1222

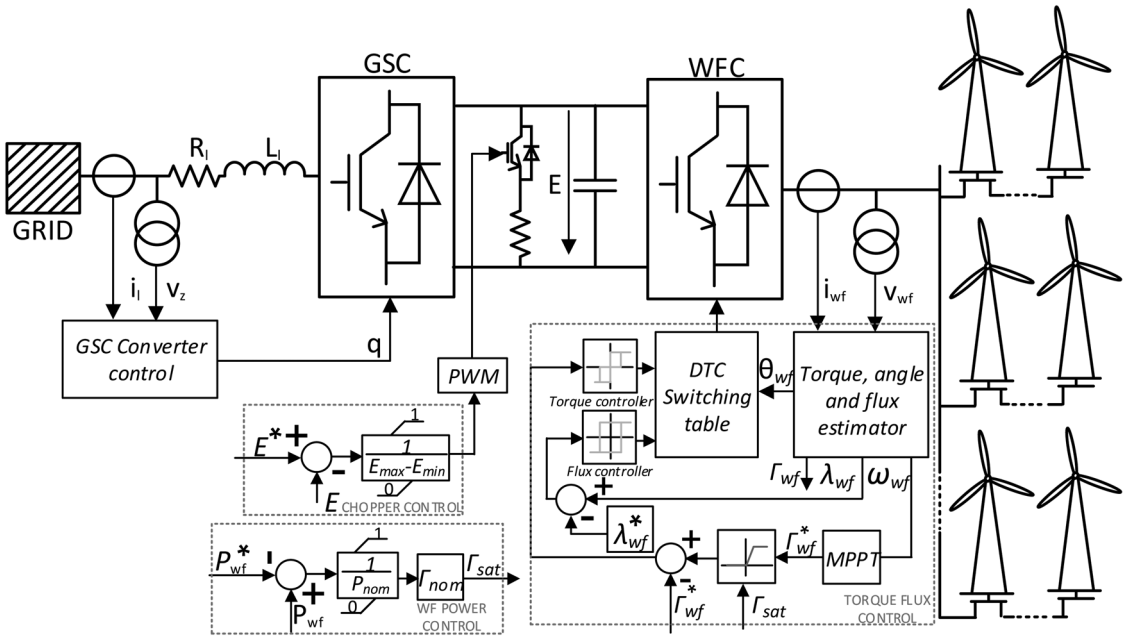

Fig. 1 *Power and control scheme of the proposed control system*

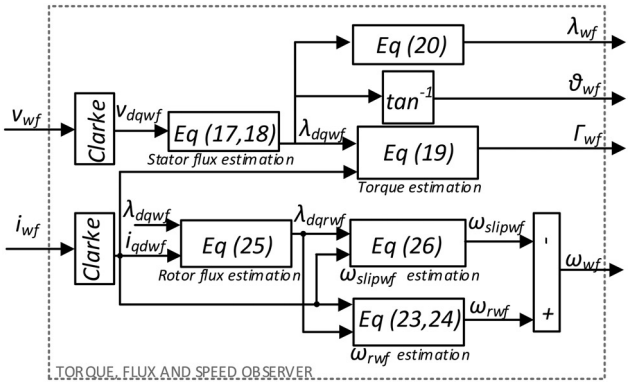

Q **Fig. 2** *Torque, flux and speed observer*

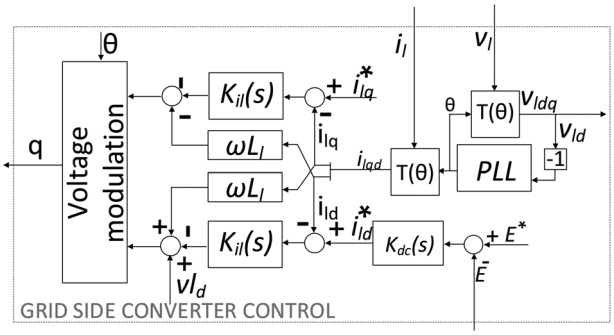

Q **Fig. 3** *GSC control scheme*

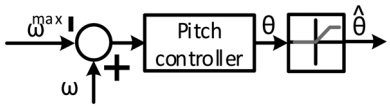

Q **Fig. 4** *Pitch angle controller*

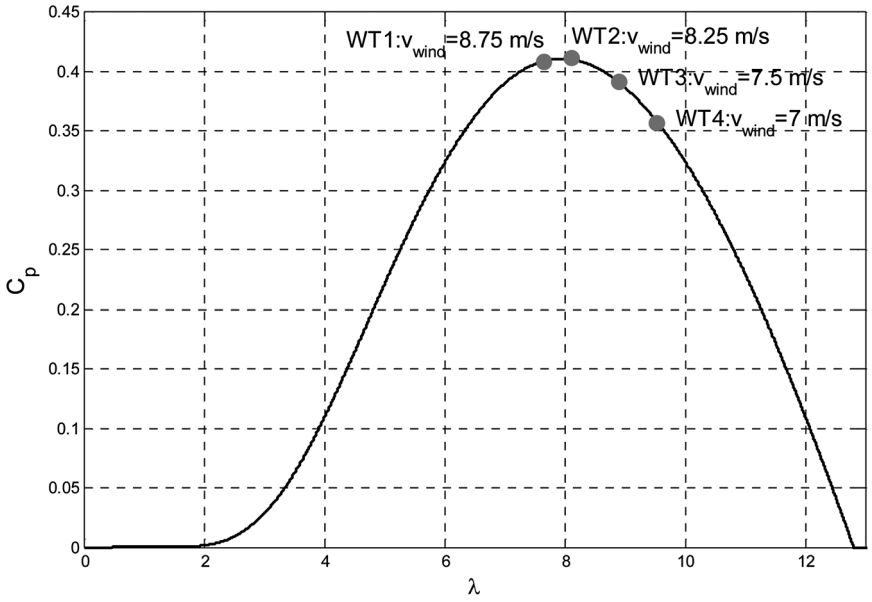

Q **Fig. 6** *Operating C_p for the different wind speeds*

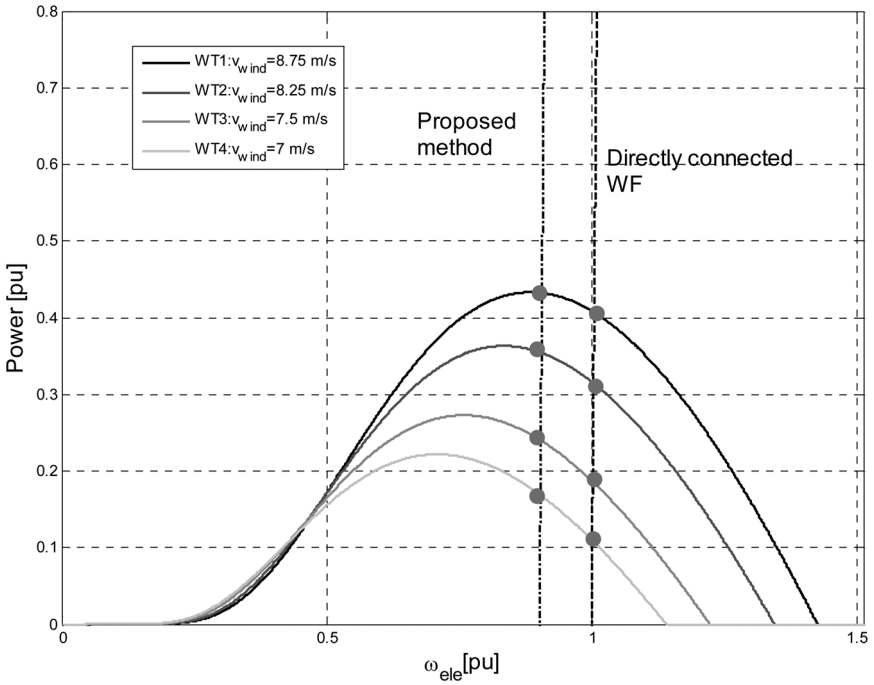

Q Fig. 7 *Power curve for the different wind turbines considering that the machines are directly connected or connected using the proposed method*

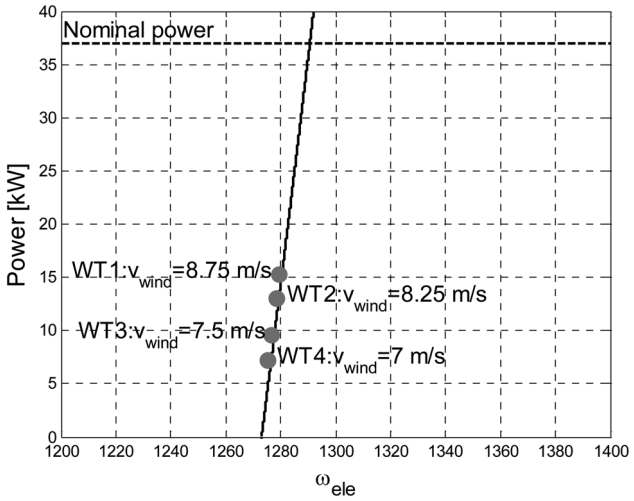

Fig. 8 *Steady-state electric characteristic of the induction machines with the operation working point for the different wind turbines*

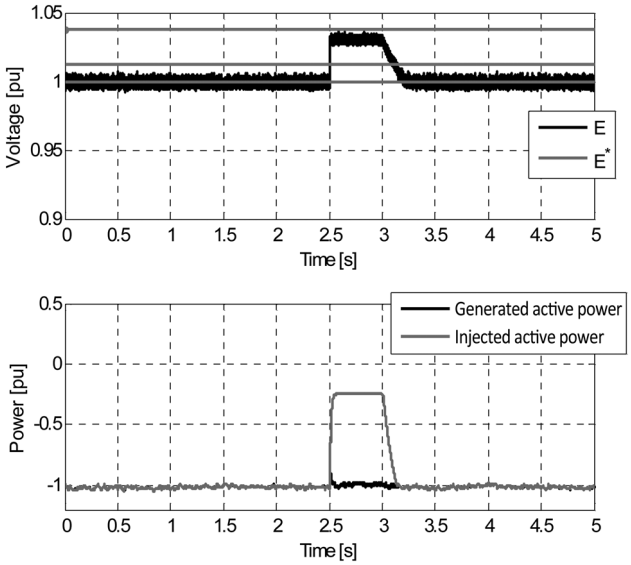

Q **Fig. 10** *DC voltage evolution (in red the minimum (E_{min}) and maximum (E_{max}) thresholds) and active power generated and injected to the grid*

RPGSI20150036_B&W

Author Queries

Agustí Egea-Alvarez, Mónica Aragüés-Peñalba, Oriol Gomis-Bellmunt,
Joan Rull-Duran, Antoni Sudrià-Andreu

Q Please make sure the supplied image is correct for both online (colour) and print (black and white), for your reference please see black and white version of image at the end of the colour proof. If changes are required please supply corrected source files along with any other corrections needed for the paper.

Q1 Please provide expansion for the abbreviation GSC, WFC, WF, PLL.

Q2 Equation (31) is appearing twice, so we have renumbered as (31a) and (31b) here and elsewhere. Please confirm the change.

Q3 We have made a change to the word 'deepness' to 'depth'. Please confirm that this is what you intended, otherwise amend it to convey your exact meaning.

Q4 Please provide volume number for Ref. [6].

Q5 As per journal style, names of up to three authors are provided. If there are more than three, only the first three should be given followed by et al. Please provide next two author names in Refs. [14, 16] as required by journal style.

Q6 Please provide page range for Ref. [18].